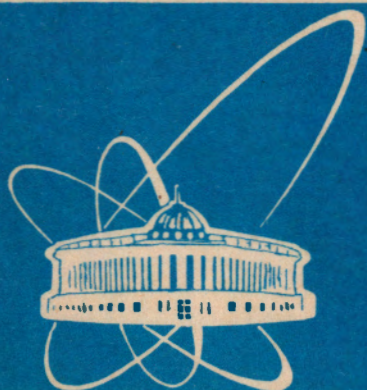


94-397



Объединенный
институт
ядерных
исследований
Дубна

E11-94-397

E.P.Zhidkov, M.B.Yuldasheva, I.P.Yudin,
O.I.Yuldashev

COMPUTATION OF THE MAGNETIC FIELD
OF A SPECTROMETER IN DETECTORS REGION

Submitted to «Nuclear Instruments and Methods-A»

1994

Introduction

Under processing of the experimental results, obtained in 1993 on the setup EXCHARM, the question was emerged about behaviour and level of magnetic field in the region where registering apparatus and targets were placed. The setup EXCHARM is a forward-spectrometer for investigation of hadron production of charmed particles and the indication of the narrow resonances in neutron-nucleus interactions on the U-70 accelerator, at IHEP, Serpukhov, near Moscow. It is a further development of spectrometer BIS-2 [1]. The spectrometer includes the following basic elements: the SP-40 magnet, proportional chambers, a charged particle identification system, a Cherenkov shower detector, scintillation hodoscopes, an electronic system for event preselection and data acquisition. The schematic view of the setup is shown in fig.1.

The spectrometer magnet is a dipole with external dimensions $450 \times 323 \times 305 \text{ cm}^3$, with aperture $100 \times 48 \text{ cm}^2$. The length of the magnet is 190 cm and the working magnitude of magnetic field is 0.75 T . The schematic picture of the magnet is shown in fig.2.

The Cherenkov shower detector-hodoscope is proposed for the registration and identification of electrons, positrons and gamma-quanta.

The proportional chambers are used for track reconstruction of the particles. Identification of charged particle momentum is very important problem and its solving is based on well knowledge of the magnetic field not only inside magnet but also in the region, where targets and other registering apparatus are placed. The measurements of the magnetic field components have been performed in aperture of the magnet for $-158 \text{ cm} \leq z \leq 142 \text{ cm}$. Experimental data are absent for $|z| > 158 \text{ cm}$, but this information is very interesting. For investigation of the magnetic field distribution in the region of basic detectors - proportional chambers and near target $T(z \approx 500 \text{ cm})$ the computation of the SP-40 magnetic field has been performed by code MSFE3D [2]. For computing two methods were used: the finite element method (FEM) and the FEM with suggested new infinite elements. For accuracy control the computations were carried out on a sequence of three-dimensional meshes. In this paper the computed results are given and the numerical methods are described. The performed results can be used for the field behaviour estimate of similar spectrometer magnets.

1 Using the finite element method

We consider the differential formulation of the magnetostatic problem for two scalar potentials [3], total - ψ and reduced - ϕ . Let Ω_F be a region with ferromagnetic material. We choose some region Ω , which contains Ω_F . Let Γ_0 be a boundary of the region Ω and $\Omega_A = \Omega \setminus \Omega_F$. Γ is a boundary between Ω_F and Ω_A . Then we have equations

$$\text{div}(\mu \nabla \psi) = 0, \quad x \in \Omega_F; \quad (1)$$

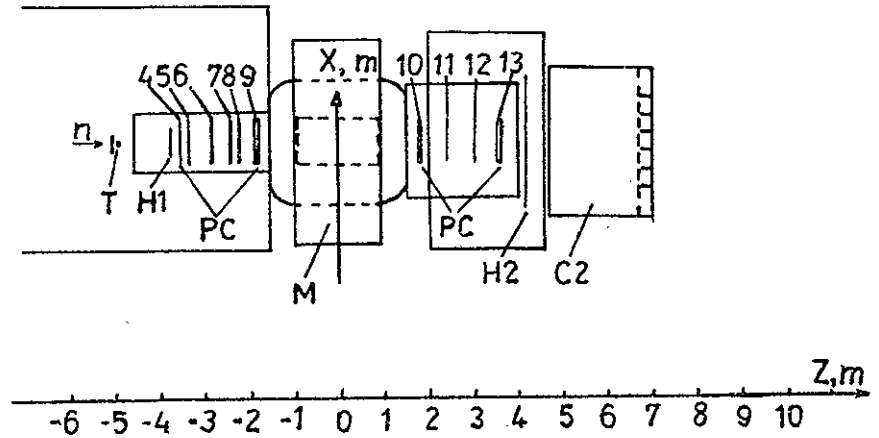


Fig.1. Schematic view of the setup. PC: proportional chambers; M: magnet SP-40; T: target; H1,H2: hodoscopes of scintillation counters; C2: Cherenkov shower detector-hodoscope

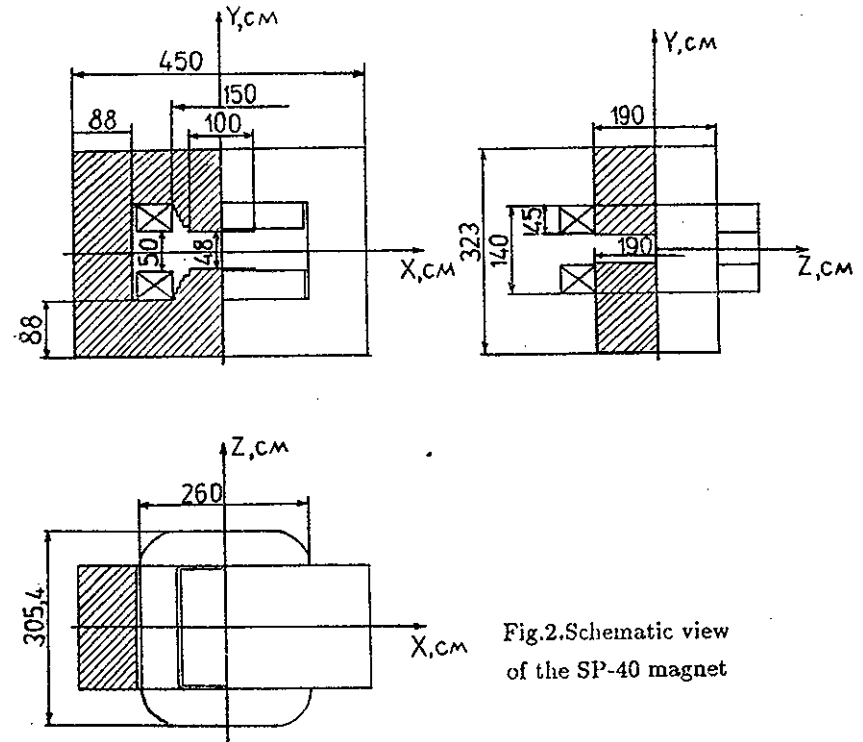


Fig.2. Schematic view of the SP-40 magnet

$$\operatorname{div}(\nabla\phi) = 0, \quad x \in \Omega_A; \quad (2)$$

with the boundary conditions

$$\mu(\partial\psi/\partial n) = \partial\phi/\partial n - \mathbf{n} \cdot \mathbf{H}^S, \quad x \in \Gamma; \quad (3)$$

$$\psi = \phi + \phi^S, \quad x \in \Gamma; \quad (4)$$

$$\phi \approx 0, \quad x \in \Gamma_0. \quad (5)$$

Function $\mu = \mu(|\nabla\psi|)$ is given from the closed interval $1 \leq \mu_* \leq \mu \leq \mu^*$ where μ_* and μ^* are known constants. Vector \mathbf{H}^S is computed by the Biot-Savart's law

$$\mathbf{H}^S(x_0) = \frac{\mu_0}{4\pi} \int_{\Omega_S} \mathbf{J} \times \nabla \frac{1}{|x - x_0|} d\Omega_S,$$

where Ω_S is a source region, \mathbf{J} is a known vector of current density, μ_0 is the permeability of free space, $|x - x_0|$ is the distance between points x and x_0 . Potential ϕ^S is defined from the Laplace equation in the region Ω_F

$$\Delta\phi^S(x) = 0, \quad x \in \Omega_F, \quad (6)$$

with the boundary conditions

$$\frac{\partial\phi^S}{\partial n} = -\mathbf{n} \cdot \mathbf{H}^S, \quad x \in \Gamma, \quad \int_{\Gamma} \mathbf{n} \cdot \mathbf{H}^S ds = 0. \quad (7)$$

It is known that the generalized solutions of the formulated boundary value problems exist. The generalized solution of nonlinear problem (1) - (5) is unique, and the generalized solution of Neumann problem (6) - (7) is defined with constant. Finite element approximations converge to the exact generalized solutions. As a finite element $\bar{\Omega}_j$, we choose convex hexahedron. Let us divide Ω by the finite elements so that $\bar{\Omega} = \cup \bar{\Omega}_j$, $\Omega_i \cap \Omega_j = \emptyset$, when $i \neq j$, supposing also, that every face of element $\bar{\Omega}_j$ is either a subset of Γ_0 , or a face of the other element, and the boundary Γ is formed by faces of the chosen elements.

We introduce in space with Cartesian coordinate system related to variable $\xi = (\xi_1, \xi_2, \xi_3)$, the linear shape functions N_m^e for cube $[-1, 1]^3$

$$N_m^e(\xi) = (1/8)(1 + \sigma_{m1}\xi_1)(1 + \sigma_{m2}\xi_2)(1 + \sigma_{m3}\xi_3), \quad m = 1, \dots, 8,$$

where the coefficients σ_{mk} are chosen as 1 or -1 so that N_m^e is equal to 1 in the vertex with number m and 0 in any other vertex. In view of that the cube $[-1, 1]^3$ turns into the element $\bar{\Omega}_j$ under the use of the transformation

$$x_k = \sum_{m=1}^8 x_k^{j,m} N_m^e(\xi), \quad k = 1, 2, 3,$$

where $x_k^{j,m}$, $k = 1, 2, 3$ are coordinates of the element $\bar{\Omega}_j$ vertex with number m , the base functions $N_m(\xi(x))$, $m = 1, \dots, 8$ on element $\bar{\Omega}_j$ may be obtained. We shall find the solutions of the problems (1)-(5) and (6)-(7) in the form

$$\psi(x) = \sum_j \psi_j N_i(x), \quad x \in \bar{\Omega}_F;$$

$$\phi(x) = \sum_j \phi_j N_j(x), \quad x \in \bar{\Omega}_A; \quad (8)$$

$$\phi^S(x) = \sum_j \phi_j^S N_j(x), \quad x \in \bar{\Omega}_F,$$

where $\psi_j, \phi_j, j = 1, \dots, M$ and $\phi_j^S, j = 1, \dots, M_S$ are unknown potentials values in nodes of the space mesh, which is obtained as a result of partitioning the region $\bar{\Omega}$. Substituting the expressions for ψ and ϕ from (8) into generalized formulation of problem (1)-(5) and taking the boundary conditions into account, we perform the equation

$$\begin{aligned} \sum_{x^j \in \bar{\Omega}_F} \psi_j \int_{\Omega_F} \mu \nabla N_i \cdot \nabla N_j d\Omega + \sum_{x^j \in \Gamma} \psi_j \int_{\Omega_A} \nabla N_i \cdot \nabla N_j d\Omega + \sum_{x^j \in \Omega_A} \phi_j \int_{\Omega_A} \nabla N_i \cdot \nabla N_j d\Omega = \\ = - \int_{\Gamma} N_i \mathbf{n} \cdot \mathbf{H}^S dS + \sum_{x^j \in \Gamma} \phi_j^S \int_{\Omega_A} \nabla N_i \cdot \nabla N_j d\Omega, \end{aligned} \quad (9)$$

$$j = 1, \dots, M.$$

Potential ϕ^S is found from the equation

$$\sum_{x^j \in \bar{\Omega}_F} \phi_j^S \int_{\Omega_F} \nabla N_i \cdot \nabla N_j d\Omega = - \int_{\Gamma} N_i \mathbf{n} \cdot \mathbf{H}^S dS, \quad (10)$$

$$j = 1, \dots, M_S.$$

Note that there is no need to solve this equation in whole Ω_F , because $\mathbf{H}^S = -\nabla\phi^S$ is orthogonal to gradients of the functions which are equal to 0 on the boundary of Ω_F [4]. I.e. it is enough to solve equation (10) in some situated near boundary volume of the region, completing the boundary conditions.

The integrals over regions Ω_F, Ω_A in (9) - (10) are computed by summation of the contributions from separate elements $\bar{\Omega}_j$. In such an element μ is a constant, its argument is computed in the centre. The centre is the point, every coordinate of which is the arithmetic mean of coordinates of hexahedron vertices.

Let us write the discretized system of the nonlinear algebraic equations (9) with sparse matrix as

$$F(\mu)y = f, \quad \mu = \mu(y). \quad (11)$$

Usually for solving such a system some linearization is used and then the finding of the solution of system (11) reduces to the sequential solving of the linear problems. General iterative scheme for solving the nonlinear equation (11) has the form

$$B_n \frac{y_{n+1} - y_n}{\tau_n} = -(F_n y_n - f), \quad n = 0, 1, \dots, \quad (12)$$

where y_0, F_0, τ_0 are given. Two kinds of this process are usually used:

1. $B_n = F_n, \tau_n \equiv 1$;
2. $B_n = F'_n$, where F'_n is Jacobi matrix.

We use iterative scheme (12) for $B_n \equiv F_n$ and $\tau_n \in (0, 1]$. The parameter τ_n is chosen depending on behavior of μ on every iteration. Note that the general theory of the iterative process (12) for self-adjoint, positive definite operator F is given in book [5].

Independently of B_n form, the linearized system of equations on every iteration should be solved

$$Az = b, \quad (13)$$

where A - symmetric, positive definite sparse matrix. Usually for this purpose the incomplete Cholesky decomposition with conjugate gradient method is used [6]. The special algorithms developed by authors in [7] are used for solving the equation (13) on the vector computer CONVEX C120.

2 Infinite elements

Let us use a more exact boundary condition than approximation (5). Let

$$\lim_{x \rightarrow \infty} \phi = 0, \quad (14)$$

i.e. the solution region of the problem extends to infinity. Usually in such cases infinite elements or boundary equations methods are used or the problem is formulated in volume integral equation form [8]. There are some approaches to construct infinite elements [9]. We shall use the fact that for the Laplace equation in spherical coordinate system the solution of the Dirichlet problem has, for example, [10], the known form

$$\phi(r, \theta, \varphi) = \sum_{n=0}^{\infty} \frac{\gamma_n}{r^{n+1}} Y_n(\theta, \varphi), \quad (15)$$

where spherical functions Y_n are given by the formulas

$$Y_n(\theta, \varphi) = \sum_{k=0}^n (\alpha_{nk} \cos k\varphi + \beta_{nk} \sin k\varphi) P_n^{(k)}(\cos \theta), \quad (16)$$

here $P_n^{(k)}$ are associated Legendre functions.

Let us circumscribe around the magnetic system some sphere with radius r_0 , the centre of the sphere is the same as the centre of the magnetic system. It is known, for example, [10], that for harmonic function ϕ the following behaviour is valid

$$\phi(x) \sim O\left(\frac{1}{|x|^2}\right) \text{ when } |x| \rightarrow \infty,$$

under the condition

$$\int_{\Gamma} \frac{\partial \phi}{\partial n} d\Gamma = 0,$$

where Γ is the surface of the sphere.

For required solution outside of this sphere the representation

$$\phi(r, \theta, \varphi) = \sum_{n=1}^{\infty} \left(\frac{r_0}{r}\right)^{n+1} Y_n(\theta, \varphi),$$

is correct. Function $Y_0 = 0$ in view of symmetry of the magnetic system, the coefficients α_{nk} and β_{nk} have the form:

$$\alpha_{nk} = \frac{(2n+1)(n-k)!}{2\pi(n+k)!} \int_0^{2\pi} \int_0^{\pi} \phi(r_0, \theta, \varphi) P_n^k(\cos \theta) \cos k\varphi \sin \theta d\theta d\varphi,$$

$$\beta_{nk} = \frac{(2n+1)(n-k)!}{2\pi(n+k)!} \int_0^{2\pi} \int_0^{\pi} \phi(r_0, \theta, \varphi) P_n^k(\cos \theta) \sin k\varphi \sin \theta d\theta d\varphi.$$

Note that every element of the sphere surface may correspond to the element of a cube surface, including the sphere and having the common centre with it.

As infinite elements, we consider infinite regions formed by the rays, starting from rectangular elements of the cube surface and which are extension of the rays, starting from the sphere centre. In every such an infinite element the solution has the form (15). Find the approximation for solution $\phi(r, \theta, \varphi)$ convenient for numerical realization. Consider the case, when a cube face is the part of plane $x_3 = L \equiv \text{const}$. The other cube faces are considered by analogous approach.

For the rectangular element of the chosen face, when $x_i^a \leq x_i \leq x_i^b, i = 1, 2$, we have

$$\phi(x_1, x_2, L) = \sum_{k=1}^4 \phi(x_1^k, x_2^k, L) (a_k x_1 + b_k x_2 + c_k x_1 x_2 + d_k) + O(\delta_1^2 + \delta_2^2), \quad (17)$$

where according to bilinear representation

$$a_k = \frac{\kappa_{k1}}{2\delta_1} \left(1 - \frac{\kappa_{k2}}{\delta_2} S_2\right), \quad b_k = \frac{\kappa_{k2}}{2\delta_2} \left(1 - \frac{\kappa_{k1}}{\delta_1} S_1\right),$$

$$c_k = \frac{\kappa_{k1} \kappa_{k2}}{\delta_1 \delta_2}, \quad d_k = \frac{a_k b_k}{c_k}.$$

Here for $i = 1, 2$ the notations

$$\delta_i = x_i^b - x_i^a, \quad S_i = x_i^b + x_i^a,$$

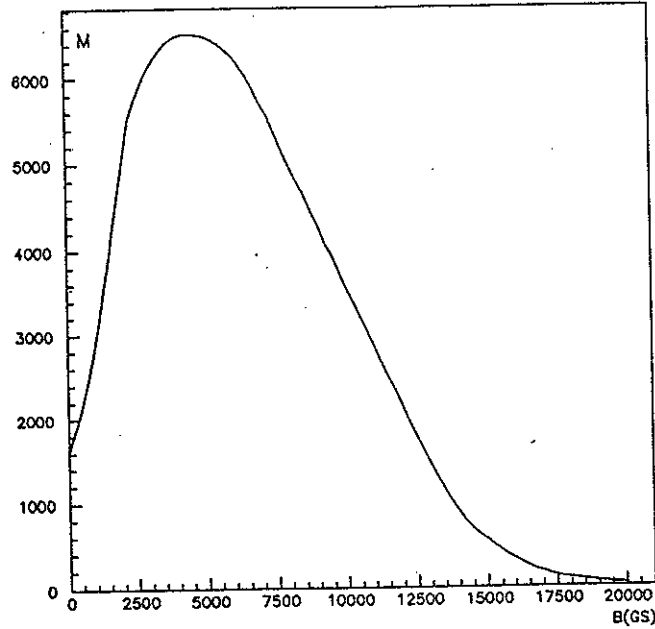


Fig.3. Function $\mu(|\vec{B}|)$

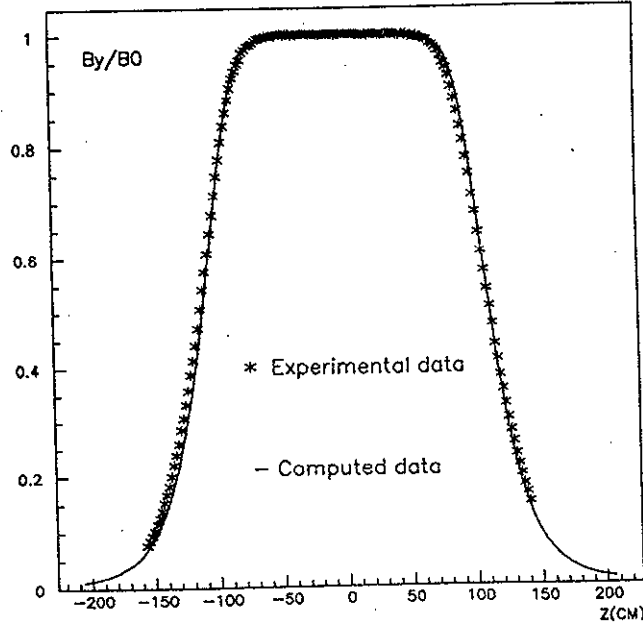


Fig.4. The comparison of computed and experimental data for relative field component B_y/B_0 , for $x=0$ cm, $y=1$ cm

are used. Coefficients κ_{ki} are chosen as 1 or -1 so that the bilinear function

$$M_k^e = a_k x_1 + b_k x_2 + c_k x_1 x_2 + d_k$$

is equal to 1 in the vertex of the rectangular element with number k and 0 in other its vertices.

On the other hand, according to (15),(16) for the infinite element we have:

$$\begin{aligned} \phi(r, \theta, \varphi) = & \frac{\gamma_1}{r^2} (\alpha_{10} \cos \theta + \alpha_{11} \sin \theta \cos \varphi + \beta_{11} \sin \theta \sin \varphi) + \\ & + \frac{\gamma_2}{r^3} \beta_{22} 3 \sin^2 \theta \sin 2\varphi + O\left(\left(\frac{1}{r}\right)^3\right). \end{aligned} \quad (18)$$

Let

$$r_a = L / \cos \theta,$$

then from the condition of function continuity on the cube face as in form (15), and as in form (17), we get:

$$\begin{aligned} \gamma_1 = r_a^3, & \quad \gamma_2 = r_a^5, \\ \alpha_{10} = (1/L) \sum_{k=1}^4 \phi_k d_k, & \quad \alpha_{11} = \sum_{k=1}^4 \phi_k a_k, \\ \beta_{11} = \sum_{k=1}^4 \phi_k b_k, & \quad \beta_{22} = (1/6) \sum_{k=1}^4 \phi_k c_k. \end{aligned}$$

Substituting the obtained coefficients into (18) and using the notations

$$r_a \cos \varphi \sin \theta = (L/x_3)x_1, \quad r_a \sin \varphi \sin \theta = (L/x_3)x_2,$$

we have the following approximation for infinite element:

$$\phi(x) \approx \sum_{k=1}^4 \phi_k \left((L/x_3)^3 a_k x_1 + (L/x_3)^3 b_k x_2 + (L/x_3)^5 c_k x_1 x_2 + (L/x_3)^2 d_k \right).$$

For the other cube faces we have

$$\phi(x) \approx \sum_{k=1}^4 \phi_k \left((L/x_2)^3 a_k x_1 + (L/x_2)^3 b_k x_3 + (L/x_2)^5 c_k x_1 x_3 + (L/x_2)^2 d_k \right),$$

if a cube face is the part of plane $x_2 = L \equiv const$ and

$$\phi(x) \approx \sum_{k=1}^4 \phi_k \left((L/x_1)^3 a_k x_2 + (L/x_1)^3 b_k x_3 + (L/x_1)^5 c_k x_2 x_3 + (L/x_1)^2 d_k \right),$$

if a cube face is the part of plane $x_1 = L \equiv const$.

The elements of local matrixes for infinite elements are calculated by simple analytical formulas.

Note that such an approach for construction of the base functions for infinite element allows one to raise the approximation order up to required accuracy degree.

Of course, the inclusion of infinity by infinite elements, as inclusion of any singularity, increases the matrix condition number. In such a case the use of the preconditioning with the partial Gauss block elimination for the matrix block connected with the unknowns on the cube surface is recommended. Then the matrix condition number decreases [11].

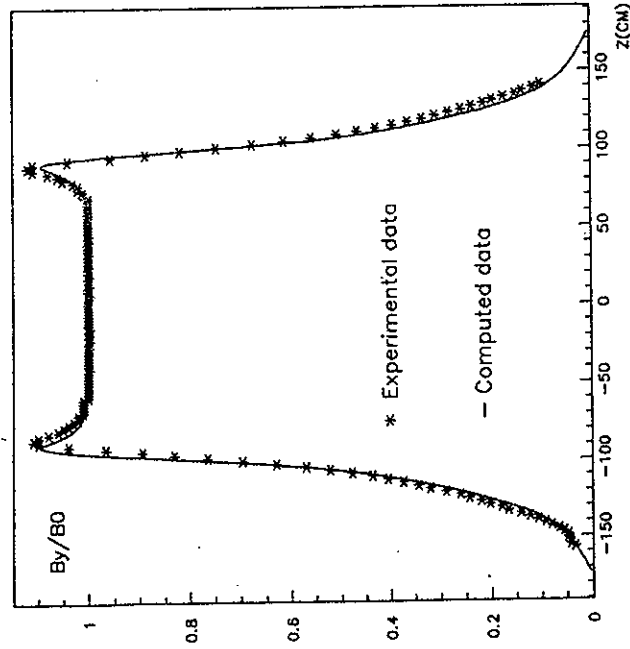


Fig.5. The comparison of computed and experimental data for relative field component B_y/B_0 , for $x=0$ cm, $y=19$ cm

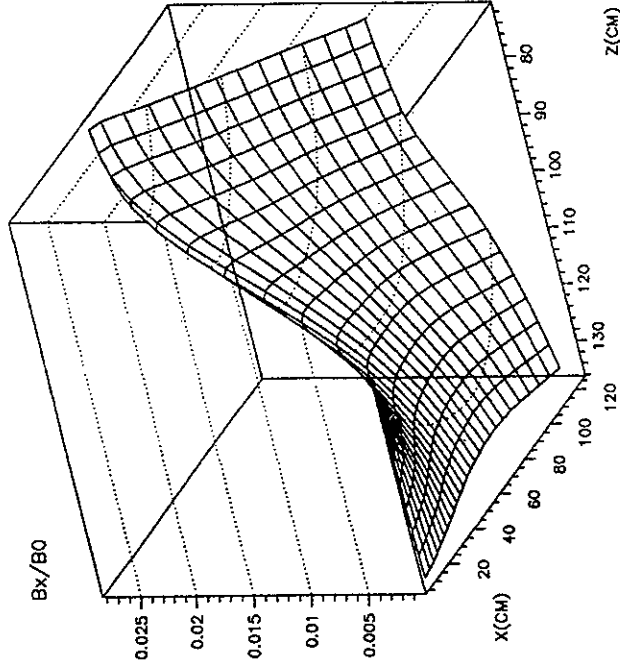


Fig.6. B_x/B_0 field component distribution at the end region of the magnet for $y=0$ cm

3 Computed results

At first for the comparison with two-dimensional computations [12], magnetic field simulation in the magnet central part has been performed by means of code MSFE3D. Supposing that the winding is long enough and the ferromagnetic core is infinite along the axis OZ , it is possible to find such a current density and a mesh in plane XOY , which ensures with high accuracy the computed results accordance with the two-dimensional computations. Farther suppose, that on the plane XOY and all other planes, which are parallel to the plane XOY and are used in computations, providing high enough accuracy meshes are chosen. Under these assumptions the investigation of the approximate solution convergence along the axis OZ has been performed. Computations were carried out on a sequence of three-dimensional meshes.

Let us present vectors \mathbf{B}_1 and \mathbf{B}_2 , obtained as the result of solving the problem on the first and the second mesh accordingly, in the form

$$\mathbf{B}_1 = P_1 \mathbf{B}^* + P_1 \bar{\delta}(h_1^{(1)}, h_2^{(1)}, \dots, h_m^{(1)}),$$

$$\mathbf{B}_2 = P_2 \mathbf{B}^* + P_2 \bar{\delta}(h_1^{(2)}, h_2^{(2)}, \dots, h_m^{(2)}),$$

where P_1 and P_2 are the operators, projecting continuous vector-functions on the first and the second mesh; $\bar{\delta}$ is the error vector-function, h_1^i, \dots, h_m^i , $i = 1, 2$ are the meshes parameters of the quasiuniform partitions of these two meshes along the axis OZ . It means that the region along this direction is divided into $m - 1$ elements, in every of which the partition with the step h_k^i , $1 \leq k \leq m$ is carried out for $i = 1, 2$.

Suppose that the approximate relation is valid:

$$\bar{\delta}(h_1, \dots, h_m) \approx C_1 \bar{h} + O(\bar{h}^2), \text{ where } \bar{h} = (\sum_{k=1}^m h_k) / m.$$

Then for main error member we have approximate estimates on the first and the second mesh:

$$(\mathbf{B}_1 - P_1 \mathbf{B}_2) \frac{\bar{h}^{(1)}}{\bar{h}^{(1)} - \bar{h}^{(2)}} \approx P_1 C_1 \bar{h}^{(1)}$$

$$(P_2 \mathbf{B}_1 - \mathbf{B}_2) \frac{\bar{h}^{(2)}}{\bar{h}^{(1)} - \bar{h}^{(2)}} \approx P_2 C_1 \bar{h}^{(2)}.$$

Our calculations have shown that already for two meshes having 32000 and 42800 nodes the estimate for the main error member is not more than $6 \cdot 10^{-3}$.

All computed results are presented here in figures as the relations to the required magnetic field value B_0 in the magnet centre, where B_0 is equal to 0.75 T. The comparison of the computed (42800 nodes) and experimental curves for the relative main field component $B_y(z)/B_0$, has shown (fig.4) that inside the magnet the difference is not more than $\approx 10^{-3}$. In this case the current is 144308 A. In fig.5 the computed and experimental results are presented for the relative main component of the magnetic field for $x = 0$ cm., $y = 19$ cm.

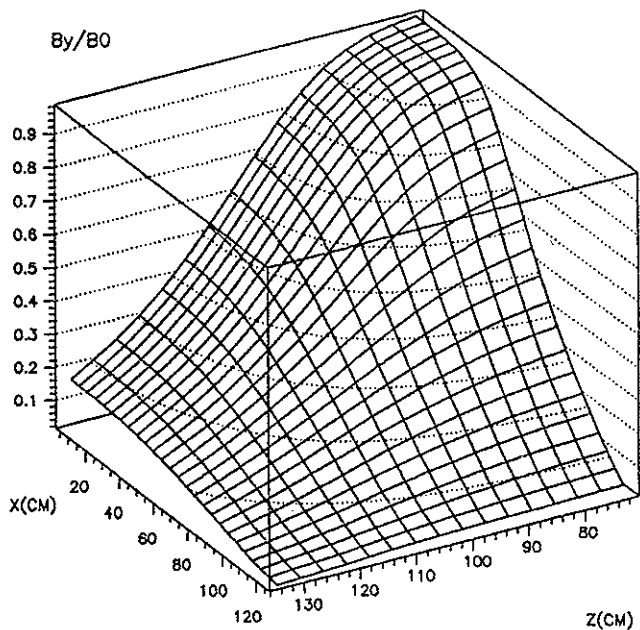


Fig.7. B_y/B_0 field component distribution at the end region of the magnet for $y=0$ cm

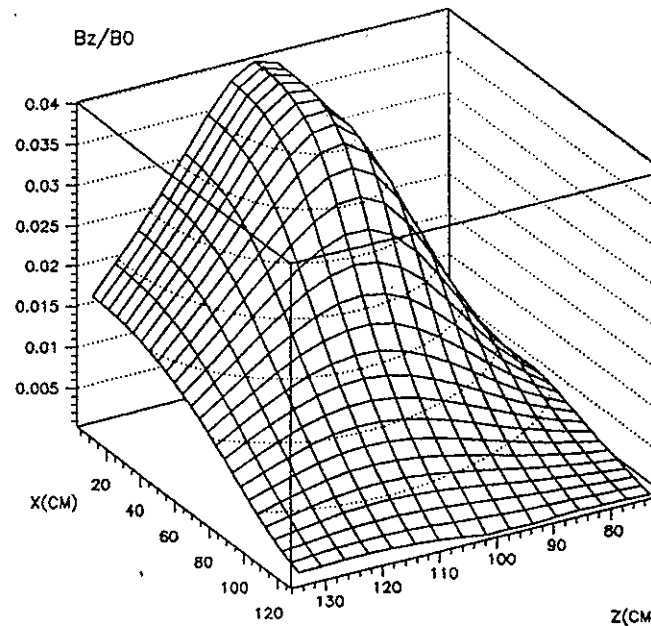


Fig.8. B_z/B_0 field component distribution at the end region of the magnet for $y=0$ cm

In figs.6-8 the field components at the end region of the magnet are given for $y = 0$ cm. The computations have shown that the absolute values of the field components B_x/B_0 and B_z/B_0 in this region are not more than 2,7 % and 4 % accordingly.

In figs.9-16 the relative field components behaviour in the basic detectors (proportional chambers) region is presented. The computations have been performed on the finite element mesh having 51840 nodes. As in these figures the difference between the computed results obtained by the FEM and by the FEM with the infinite elements method is not practically observed, the field behaviour obtained by the second method only is given here.

In figs.9-12 the relative main field component B_y/B_0 behaviour in dependence on x and z under the different values of y on boundaries of the detectors region is presented.

In figs.13,14 the relative component B_x/B_0 in dependence on x for $z = 167.5$ cm and in dependence on z for $x = 93.6$ cm under the different values of y is given.

In figs.15,16 the relative component B_z/B_0 in dependence on x and on z is shown.

As it is clear from these figures, all field components are smooth functions and rapidly decreasing with growth of z . With the growth of y the main field component changes the sign. The represented figures can be used for the field behaviour estimates of similar spectrometer magnets.

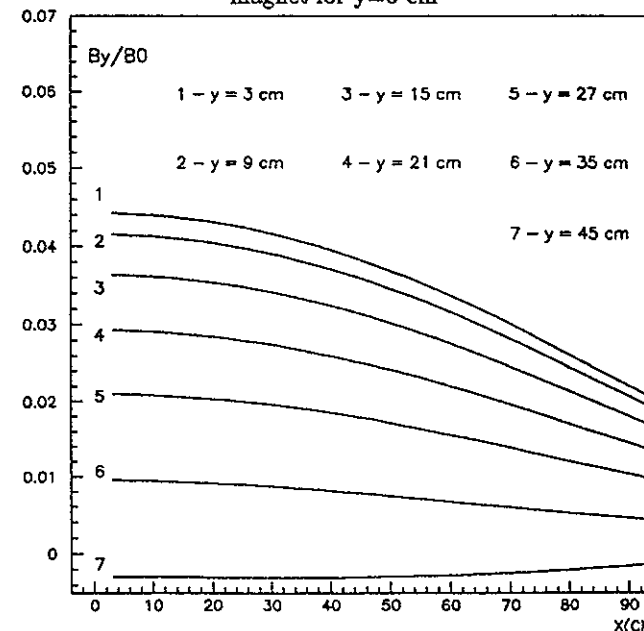


Fig.9. B_y/B_0 field component distribution for $z=167.5$ cm

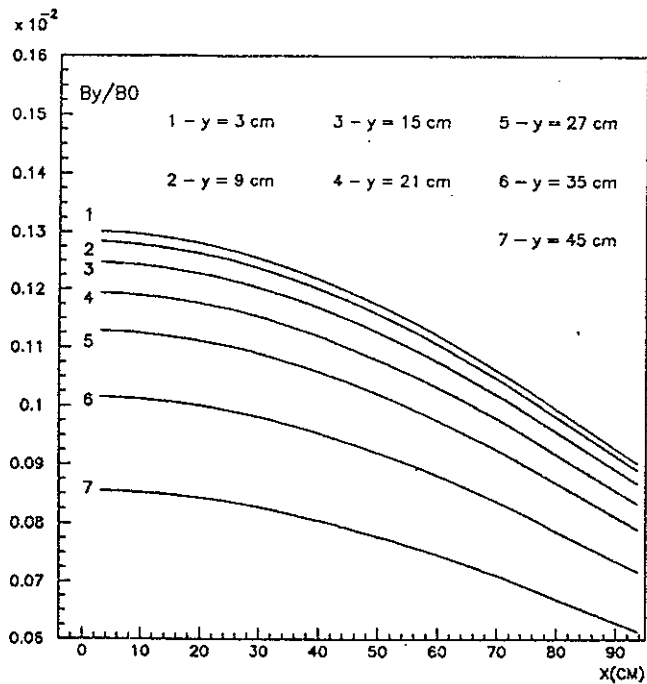


Fig. 10. B_y/B_0 field component distribution for $z=293.8$ cm

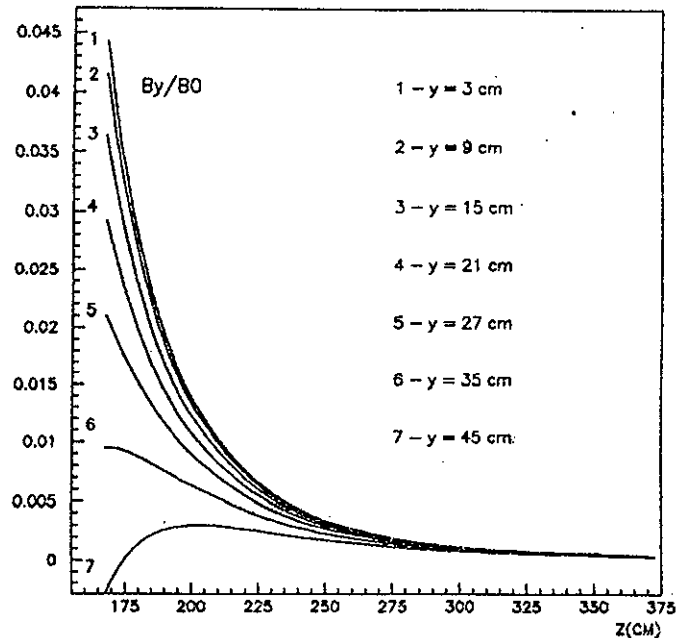


Fig. 11. B_y/B_0 field component distribution for $x=3.125$ cm

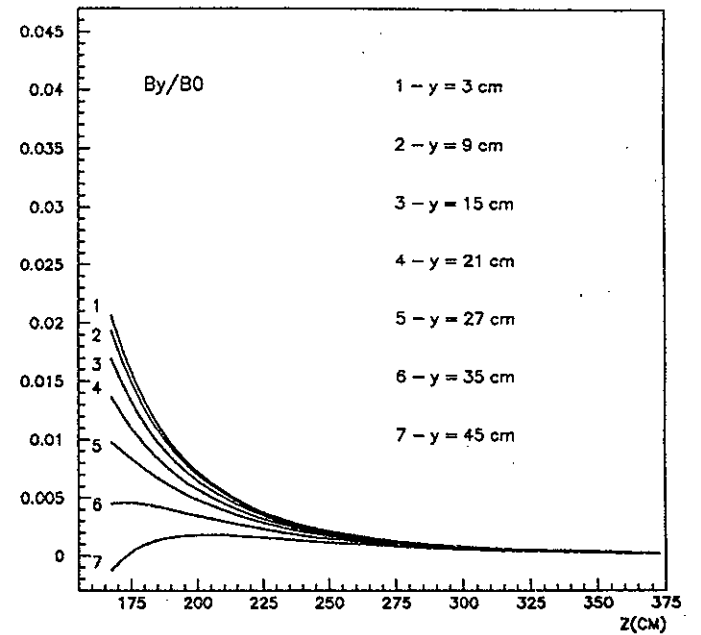


Fig. 12. B_y/B_0 field component distribution for $x=93.6$ cm

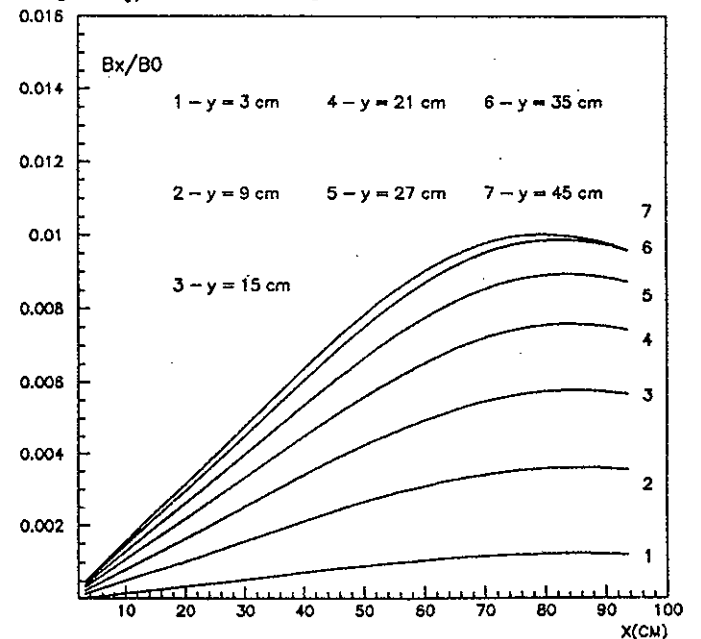


Fig. 13. B_x/B_0 field component distribution for $z=167.5$ cm

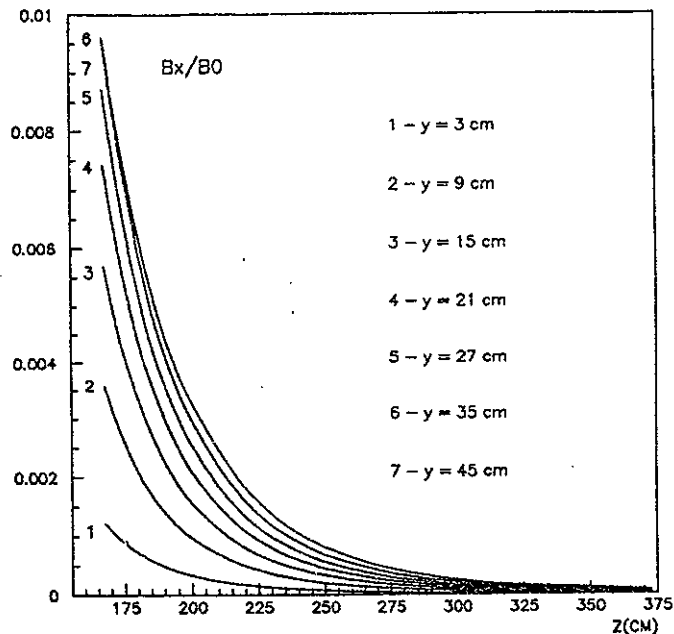


Fig.14. B_x/B_0 field component distribution for $x=93.6$ cm

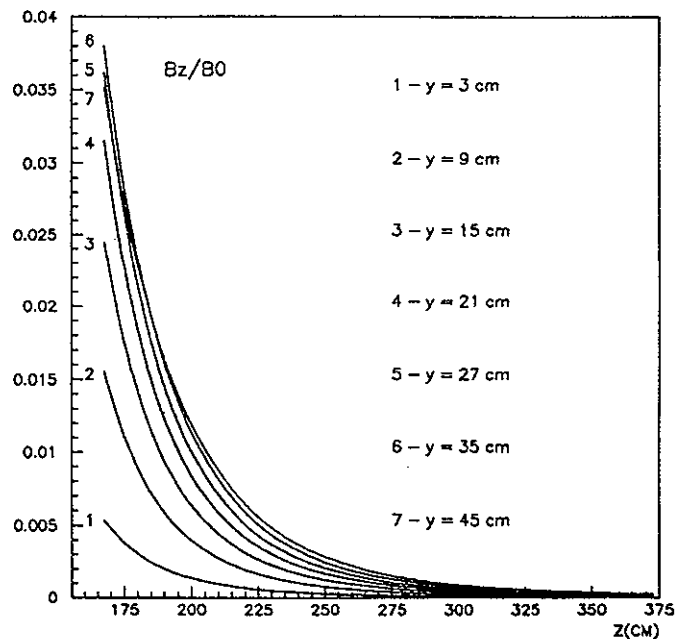


Fig.16. B_z/B_0 field component distribution for $x=3.125$ cm

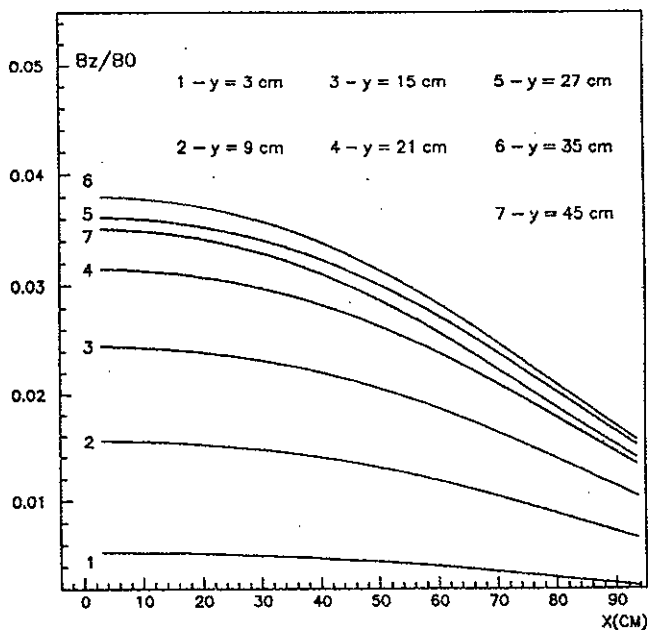


Fig.15. B_z/B_0 field component distribution for $z=167.5$ cm

Acknowledgments. Authors wish to express gratitude to Professor I.A.Savin and Professor V.D.Kekelidze for attention and encouragement of the work, Dr. D.A.Kirillov - for submitted experimental data, Mr. V.A.Panacik and Mrs. N.V.Chernenko - for the help in some computed results processing. E.P.Zhidkov and O.I.Yuldashev thank the Russian Fund of Fundamental Investigations (grant N 94-01-01354-a) for support.

References

- [1] A.N.Aleev et al., JINR, P1-89-854, Dubna (1989).
- [2] M.B.Yuldasheva, O.I.Yuldashev, JINR, P11-94-202, Dubna (1994).
- [3] J.Simkin, C.W.Trowbridge, Proc. IEE, 127, Pt. B (1980) 368.
- [4] E.P.Zhidkov, M.B.Yuldasheva, I.P.Yudin, O.I.Yuldashev, JINR, P11-94-160, Dubna (1994).

- [5] A.A.Samarskii, E.S.Nikolaev, Methods of Solving the Mesh Equations, (Nauka, Moscow, 1978).
- [6] J.A.Meijerink, H.A.van der Vorst, Math. Comp., 31 (1977) 148;
D.S.Kershaw. J. of Comp. Physics., 26 (1978) 43.
- [7] E.P.Zhidkov, M.B.Yuldasheva, O.I.Yuldashev, JINR, P11-94-161, Dubna (1994).
- [8] A.A.Airyany, E.P.Zhidkov et al., EChAYa. 21 (1990) 251
- [9] P.Bettess, IEEE Trans. on Mag., 24 (1988) 238.
- [10] Collection of Exercises on Mathematical Physics Equations,
ed. V.S.Vladimirov, (Nauka, Moscow, 1982).
- [11] J.Mandel, Numer. Math., 58 (1990) 79.
- [12] E.P.Zhidkov, S.Lima, R.V.Polyakova, I.P.Yudin, JINR, P11-92-490, Dubna (1992).

Received by Publishing Department
on October 13, 1994.